High-Accuracy Schottky Diagnostics for Low-SNR Betatron Tune Measurement in Ramping Synchrotrons

Pei-han Sun,[1,2,*] Man-zhou Zhang,[1,3,†] Ren-xian Yuan,[1,3] De-ming Li,[1] Jian Dong,[3] and Ying Shi[1,2]

[1]*Shanghai Institute of Applied Physics, Chinese Academy of Sciences, Shanghai 201800, China*
[2]*University of Chinese Academy of Sciences*
[3]*Shanghai Advanced Research Institute, Chinese Academy of Sciences, Shanghai 201204, China*

This study introduces a novel real-time betatron tune measurement algorithm, utilizing Schottky signals and an FPGA-based backend architecture, specifically designed for rapidly ramping synchrotrons, with particular application to the Shanghai Advanced Proton Therapy (SAPT) facility. The developed algorithm demonstrates improved measurement accuracy under challenging operational conditions, especially in scenarios with limited sampling time and signal-to-noise ratios (SNR) as low as -20 dB. By applying Short-Time Fourier Transform (STFT) analysis, the algorithm effectively accommodates the rapid increase in revolution frequency from 4 MHz to 7.5 MHz over 0.35 seconds, along with tune shifts. A macro-particle simulation methodology is employed to generate Schottky signals, which are then combined with real noise collected from an analog-to-digital converter (ADC) to simulate practical conditions. The proposed betatron tune measurement algorithm integrates advanced spectral processing techniques and an enhanced peak detection algorithm specifically tailored for low SNR conditions. Experimental validation confirms the superior performance of the proposed algorithm over conventional approaches in terms of measurement accuracy, stability, and system robustness, while meeting the stringent operational requirements of proton therapy applications. This innovative approach effectively addresses critical limitations associated with Schottky diagnostics for betatron tune measurement in rapidly ramping synchrotrons operating under low SNR conditions, laying a robust foundation and providing a viable solution for advanced applications in proton therapy and related accelerator physics fields.

Keywords: Schottky Diagnostics, Betatron Tune Measurement, SAPT

I. INTRODUCTION

To optimize the third-order resonance slow extraction of the SAPT facility [3], the main ring must be capable of performing betatron tune measurements under different energy and bunching or drifting beam. However, due to the absence of an integrated design for the betatron tune measurement system, the current setup can only measure the tune while bunching. Based on the practical experience of the SAPT facility, the residual oscillations after injection do not seem to be effectively sustained, making it difficult to obtain a coherent tune signal from the beam position monitor (BPM) data. This process involves using a slow extraction kicker for excitation, followed by applying a Fast Fourier Transform (FFT) to signals from the BPM. Additionally, excitation evidently interferes with the extraction process. This limitation hinders the system from meeting the demands of further optimization. Therefore, a feasible option at present is to perform tune measurements by obtaining the incoherent transverse oscillation signal, specifically using the Schottky signal measurements method.

Since the suggestion of the stochastic cooling concept by Simon van der Meer in 1969 [4], Schottky signal measurements have become a widely used non-invasive tool for determining beam properties, including momentum spread, betatron tune, synchrotron frequency, and chromaticity. In practice, achieving a high SNR has consistently proven to be challenging. The SNR of the measured signal is influenced by factors such as the longitudinal length of the pick-up, the sensitivity of the BPM, and the operating frequency of the system. As a result, the design and manufacturing of the pick-up may be constrained by various factors, complicating efforts to ensure a high SNR. Given these limitations, an alternative approach is necessary for measuring the betatron tune at the SAPT facility.

This paper outlines the method and procedure for measuring the betatron tune under conditions of low SNR and fluctuating betatron tune. We incorporate simulated signals—both with and without coherent components—at varying revolution frequencies and betatron tunes, combined with real-world noise collected from an analog-to-digital converter (ADC), to evaluate the reliability and general applicability of this method. Depending on signal quality and specific requirements, various spectral smoothing techniques can be employed to balance processing time and precision.

The paper is organized as follows: Section II provides method of the time-domain Schottky signal simulation, including a comparison between the Monte Carlo-based simulation method and the beam dynamics-based simulation method. Section III introduces a key innovation of this paper: an enhanced peak-detection algorithm specifically designed for synchrotrons operating under low signal-to-noise ratio (SNR) conditions during bunching or beam drifting. The method begins with a detailed data preprocessing procedure, including analog-to-digital converter (ADC) acquisition, Short-Time Fourier Transform (STFT) window length selection, and coherent signal exclusion. This is followed by spectral processing, which involves signal folding to isolate the fixed frequency region where the transverse coherent signal is expected—a critical step for improving SNR—and subsequent smoothing. Advanced signal processing techniques

* sunpeihan22@mails.ucas.ac.cn
† Corresponding author, zhangmanzhou@sinap.ac.cn

are then integrated to enhance robustness, including Exponential Moving Average (EMA) for reference tune estimation based on historical power spectral densities (PSDs), an online median filter for shot noise reduction, Kalman filtering for multi-sensor fusion, and Weighted Linear Combination (WLC) for more accurate and reliable tune measurement. These steps collectively enable effective identification of the betatron tune under challenging conditions. In Section IV, we validate the general applicability of the proposed method under various operational scenarios. The performance of the proposed algorithm is evaluated using multiple metrics and compared with that of the conventional peak-detection algorithm. The results demonstrate that the proposed algorithm achieves superior performance in terms of accuracy, stability, and robustness under challenging conditions. Section V discusses the limitations and future work related to the validation of the proposed algorithm. Finally, concluding remarks are provided in Section VI.

II. MACRO-PARTICLE SIMULATION

A. Theoretical Background

1. Longitudinal Signal

The time-domain current signal of a single particle i circulating in the synchrotron as detected by a pickup electrode can be expressed as [1, 2]:

$$I^i(t) = q \sum_{k=-\infty}^{\infty} \delta(t - t_n - kT_0) \tag{1}$$

In a bunched beam configuration, particles execute synchrotron oscillations. The signal at the n-th harmonic can be mathematically expressed as [5–8, 15, 18]:

$$I^i(t) = \frac{\omega_0 q}{2\pi} \Re\Big(\sum_{n,p=-\infty}^{\infty} J_p\left(n\omega_0 \hat{\tau}_i\right) e^{j(n\omega_0 t + p\Omega_s t + p\psi_i)}\Big) \tag{2}$$

where:

- q is the elementary charge,
- δ is the Dirac delta function,
- t_n is the arrival time difference between particle i and the synchronous particle,
- $T_0 = \frac{1}{f_0}$ is the nominal revolution period,
- $\omega_0 = 2\pi f_0$ is the angular nominal revolution frequency in radians,
- $\hat{\tau}_i$ is the synchrotron oscillation amplitude of particle i,
- $\Omega_{s_i} = 2\pi f_{s_i}$ is the angular synchrotron frequency of particle i,
- ψ_i is the initial synchrotron phase, and
- J_p is the Bessel function of the first kind of order p.

The nominal bunch length of SAPT is about one-quarter of the circumference of the ring according to the RF voltage. The synchrotron frequency of particle i depends solely on the synchrotron oscillation amplitude and follows from the solution of the pendulum equation [8], yielding:

$$\Omega_{s_i} = \frac{\pi}{2K\left(\sin\left(\frac{\omega_{\mathrm{RF}}\hat{\tau}_i}{2}\right)\right)} \Omega_{s_0} \tag{3}$$

where $K([0,1]) \to \left[\frac{\pi}{2}, \infty\right)$ is the complete elliptic integral of the first kind, $\omega_{\mathrm{RF}} = 1 \cdot \omega_0$ is the RF frequency, and $\Omega_{s_0} = q_s \cdot \omega_0$ is the zero-amplitude synchrotron frequency, where q_s represents the synchrotron tune. The initial synchrotron phase of particle i, ψ_i, is drawn from a uniform distribution over the range $(-\pi, \pi)$.

2. Transverse Signal

The transverse Schottky signal spectra are derived from the dipole moment of the beam. For a single particle in a bunched beam within a proton synchrotron, the transverse dipole Schottky time-domain signal at the n-th harmonic can be mathematically expressed as [2, 5–7, 9, 18]:

$$D^i_{\pm q}(t) \propto \frac{\hat{x}_i}{2} \Re\Big(\sum_{n,p=-\infty}^{\infty} J_p\big((n\hat{\tau}_i \pm \frac{\hat{Q}_i}{\Omega_{s_i}})\omega_0\big) e^{j\left((n\pm Q)\omega_0 t + p\Omega_{s_i} t + p\psi_i + \phi_i\right)}\Big), \tag{4}$$

where:

- $\hat{x}_i$ is the betatron oscillation amplitude,
- q is the fractional part of the nominal fractional tune,
- $\hat{Q}_i = Q\xi\frac{\hat{p}_i}{p_0}$ is the amplitude of the tune oscillations [10], which may have any sign,
- ξ is the chromaticity,
- Q is the nominal fractional tune,
- $\hat{p}_i$ is the amplitude of momentum oscillation,
- ϕ_i is the initial betatron phase of particle i, which is also drawn from a uniform distribution over the range $(-\pi, \pi)$, similar to ψ_i.

B. Beam Dynamics Simulation

A method for constructing Schottky spectra from macro-particle simulations using the Xsuite code [2, 15] is adopted. Xsuite is a collection of Python packages designed for simulating beam dynamics in particle accelerators. It includes

Table 1. Key parameters of the SAPT facility.

Parameter	Value
Circumference	24.6 m
Intensity	1×10^{11} protons per bunch
Injection Energy	7 MeV
Extraction Energy	70–235 MeV
Tune (Injection)	$Q_x = 1.7, \quad Q_y = 1.45$
Tune (Extraction)	$Q_x = 1.68, \quad Q_y = 1.40$
Chromaticities	$\xi_x = -1.46, \quad \xi_y = -1.34$
ϵ_x, ϵ_y	2π mm·mrad
q_s	0.001
α	0.3175
Transition Gamma	$\gamma_t = 1.576$
RF Voltage	1500 V
h_{rf}	1

packages for generating and manipulating particle ensembles, as well as for single-particle tracking. By applying typical SAPT parameters, Schottky spectra at the desired energy and harmonic can be computed, as illustrated in Fig. 1.

The spectra obtained from Xsuite exhibit random fluctuations in the Schottky signal. Furthermore, the arbitrary sampling frequencies configured in the ‘xtrack.BeamPositionMonitor‘ class enable continuous recording of transverse beam positions, specifically the x- and y-centroid positions of particles, which more accurately reflect how BPM data is typically acquired in real-world scenarios. Higher sampling frequencies provide access to transverse beam oscillations at higher harmonics, which is essential for transverse Schottky diagnostics.

III. TUNE MEASUREMENT

This section presents the methodology for measuring the betatron tune. First, the data from the BPM undergoes spectral processing, as described in Section III B. Next, an enhanced peak-detection algorithm is applied to obtain accurate and stable measurement results, as detailed in Section III C. The results then undergo post-processing, discussed in Section III D. Finally, the pseudocode for the tune measurement procedure is provided in Section III E.

A. Data Preprocessing

1. ADC Acquisition and STFT Window Length Selection

A resonant stripline BPM [20–24] is currently being developed to detect the Schottky signal from SAPT. It features a bandwidth of 3 MHz, while its central frequency has yet to be determined. The detected SAPT signal will first pass through a bandpass filter to remove frequency components outside the detector’s bandwidth. The ADC acquisition will be triggered by a harmonic of the revolution frequency, which can be obtained by phase-locking an external generator to the RF frequency. This undersampling will cause the Schottky signal spectrum to alias to a predictable location. This approach eliminates the time dependence of the betatron frequency, ensuring that the transverse Schottky sideband appears in a fixed region of the spectrum. This simplifies spectral processing and the tune measurement procedure.

During operation, the proton kinetic energy increases from 70 MeV to 235 MeV, corresponding to a rise in the revolution frequency from 4 MHz to 7.5 MHz over 0.35 seconds, as shown in Fig. 2. The system is designed to measure the betatron tune across different energy levels and under both bunched and drifting beam conditions. Additionally, it must be capable of performing tune measurements during the ramping procedure, which requires automatic adaptation to revolution frequency variations at a maximum rate of 10 MHz/s or maintaining a constant revolution frequency. This constraint directly affects the sampling time, as ADC acquisition is triggered by a fixed harmonic of the revolution frequency, implying that the sampling frequency remains unchanged during data acquisition. Consequently, prolonged sampling durations can reduce frequency resolution. If the sampling duration is excessively long, the sideband location will shift, ultimately limiting the precision and accuracy of the measured tune. In the context of SAPT, a 10 kHz variation in revolution frequency during the tune measurement procedure is considered tolerable. Therefore, the window length for the STFT is set to 1 ms.

2. Coherent Signal Exclusion

In practical measurements, interference from periodic noise or coherent signals may be encountered, which can distort the desired signal. To mitigate these disturbances, the Root Mean Square (RMS) fit method is commonly employed. This approach aims to minimize the impact of noise by fitting a model to the data that best represents the underlying signal, while reducing the effect of random fluctuations.

The RMS fit procedure involves the following steps:

1. **Data Preparation**: Prepare the data collected from the ADC by ensuring it has the desired length and format for processing.

2. **Model Selection**: Choose an initial model that approximates the expected signal. This could be a sine wave, a Gaussian function, or another appropriate mathematical representation. In the context of this paper, a sine wave of the form $A\sin(2\pi f x + \phi)$ is selected.

3. **RMS Calculation**: The RMS value is computed as the square root of the mean of the squared differences between the model and the measured data. This step quantifies the goodness of the fit between the model and the data.

4. **Error Minimization**: The fitting process aims to minimize the RMS error by adjusting the parameters of the

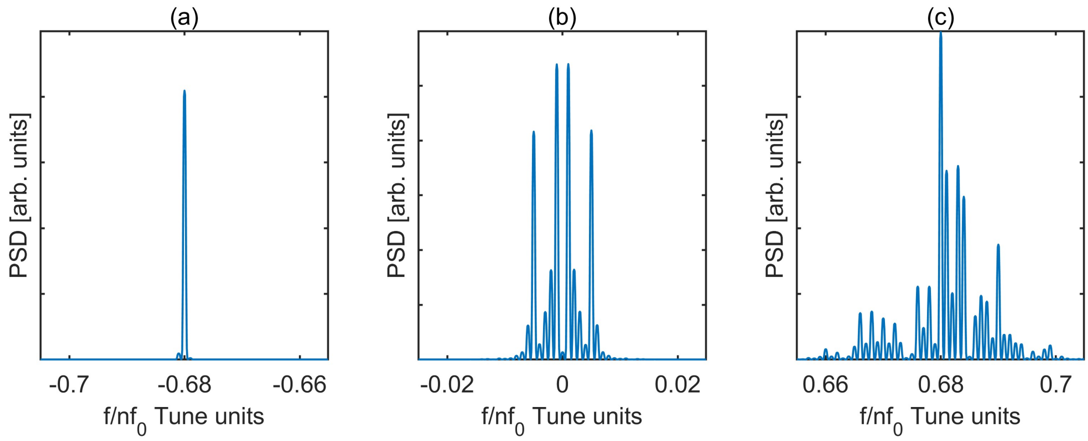

Fig. 1. Simulated PSD of the longitudinal (Fig. 1(b)) and transverse horizontal spectra (Fig. 1(a), Fig. 1(c)) for 10^{11} protons at the 5th harmonic of the revolution frequency (7.5 MHz). Typical SAPT values, as listed in Table 1, are assumed.

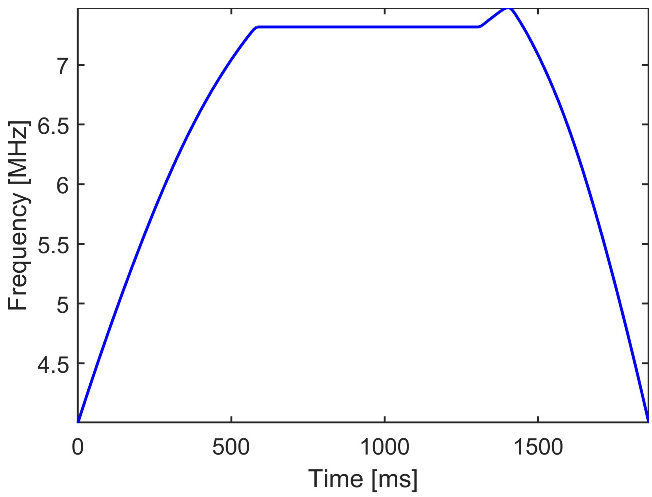

Fig. 2. Revolution frequency change during ramping and extraction process.

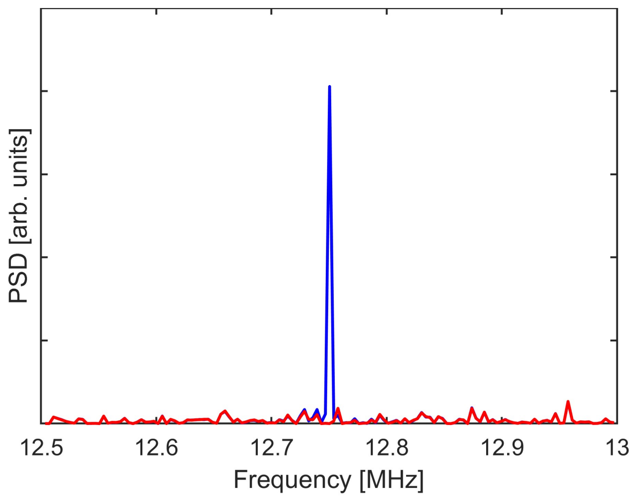

Fig. 3. Frequency-domain representation of the signal before and after the exclusion of periodic noise using the RMS fit method. The blue curve represents the original signal spectrum, while the red curve shows the spectrum with periodic noise removed.

model (e.g., amplitude, phase, frequency) until the difference between the model and the measured data is minimized.

5. **Residual Evaluation**: After the fitting procedure, the difference between the fitted model and the measured data is evaluated to ensure that the noise component has been adequately removed and that the desired signal is accurately represented.

By minimizing the RMS error, this method effectively mitigates the impact of noise, resulting in a more accurate representation of the signal, which is particularly beneficial in the analysis of Schottky diagnostics and signal preprocessing. An example of the exclusion of periodic noise from the ADC using an RMS fit is presented in Fig. 3. In practice, the coherent component in the Schottky signal can also be subtracted using this method.

B. Spectral Processing

Following the removal of the undesired coherent signal using the method outlined in Section III A 2, spectral processing techniques are employed to reduce the impact of noise power. This step is crucial to prevent spectrum degradation, facilitate accurate identification of the transverse Schottky signal's position, and enhance the SNR. Two key components of the spectral processing procedure, namely folding and smoothing, are discussed in detail in the following subsections.

1. *Folding*

In practice, due to the finite bandwidth of the BPM and the choice of sampling rates, multiple sidebands may appear

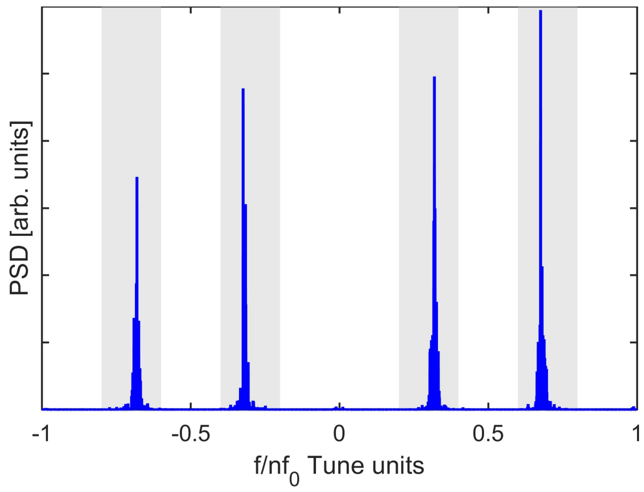

Fig. 4. The spectrum contains three revolution harmonics located at -1, 0, and 1, along with four transverse sidebands. The sidebands within the gray-shaded regions are interpolated, inverted if necessary, folded into the range $(0, 0.5)$, and averaged to improve the SNR.

in the spectrum, as shown in Fig. 4. These sidebands can be effectively utilized by interpolating and folding them into the range $(0, 0.5)$ in tune units, thereby enhancing the SNR, as demonstrated in [5] and [7]. Moreover, even if the tune shifts, the betatron tune will remain confined to a fixed region in the spectrum, provided that the sampling rate is selected as an integer harmonic of the revolution frequency. Since the bandwidth of the BPM under development is 3 MHz and the revolution frequency to be applied ranges from 4 to 7.5 MHz, only one sideband can be detected at most frequencies. Consequently, this procedure will not be used for tune measurement. However, for a wideband detector, this approach remains a feasible method for improving the SNR.

The time window for the STFT, consisting of N_t data points, is divided into multiple batches. Each batch is multiplied by a Hann window to reduce spectral leakage before being processed using the FFT. Each batch comprises N_b frequency bins. The PSD of each batch, denoted as P_{b_i}, is computed, folded, summed, and subsequently averaged to obtain $\overline{P}$.

2. *Smoothing*

To extract the transverse signal spectrum obscured by noise, Gaussian filtering is applied to $\overline{P}$ using a window of appropriate size.

When selecting the window size for filtering, manual selection reduces the method's generalizability and level of automation. A fixed-length window may have varying effects depending on the frequency resolution. At low resolution, it may excessively smooth the entire transverse signal. Therefore, the window size is determined based on the number of points in the spectrum that encompass the transverse signal spectrum.

The process begins with calculating the width of the transverse signal spectrum. For an unbunched beam, the transverse sideband width is given by

$$\Delta f_{\pm T} = f_0 \frac{\Delta p}{p} \big|(n \pm q)\eta \pm Q\xi\big|, \tag{5}$$

where η is the slip factor, and q is the fractional part of the betatron tune Q.

In the case of a bunched beam, the spectrum of a single particle splits into an infinite series of synchrotron satellites spaced by the synchrotron frequency f_s. From Equations 2 and 4, we obtain the terms $J_p\left(n\omega_0\hat{\tau}_i\right)$ and $J_p\left((n\hat{\tau}_i \pm \frac{\hat{Q}_i}{\Omega_{s_i}})\omega_0\right)$. Since $J_p(x) \approx 0$ for $p > x$, the maximum bandwidth of the transverse spectrum of a single particle is given by [12]:

$$\mathrm{BW}_{\pm T} = 2\omega_0 \Big|n\hat{\tau} \pm \frac{\hat{Q}}{\Omega_s}\Big|\Omega_s. \tag{6}$$

Therefore, for a bunched beam, the approximate width of the transverse signal spectrum at the n-th harmonic is

$$\begin{aligned} \mathrm{BW} &= \mathrm{BW}_{\pm T} + \Delta f_{\pm T} \\ &= 2\omega_0 \Big|n\hat{\tau} \pm \frac{\hat{Q}}{\Omega_s}\Big|\Omega_s + f_0 \frac{\Delta p}{p}\big|(n \pm q)\eta \pm Q\xi\big|. \end{aligned} \tag{7}$$

The maximum bandwidth of the transverse signal spectrum, denoted as $\mathrm{BW}_T = \max(\mathrm{BW})$, is computed and selected as the global width to minimize redundant calculations. Given the frequency resolution Δf, the number of spectral points encompassing the transverse Schottky signal is determined as:

$$N_T = \left\lceil \frac{\mathrm{BW}_T}{\Delta f} \right\rceil. \tag{8}$$

Experimental results under varying sampling rates and revolution frequencies indicate that optimal smoothing is achieved when the window size N_f is set to:

$$N_f = \max\left(3, 2\left\lfloor \frac{N_T}{2} \right\rfloor + 1\right). \tag{9}$$

The determined window size is then applied for smoothing, yielding the green line in Fig. 5, denoted as P_t, which represents the PSD at time t.

C. Enhanced Peak-Detection Algorithm

Previous studies have established three primary methodologies for betatron tune identification [5, 7, 9]. The first methodology, peak detection, identifies the coherent tune by locating the p-zero satellite, which serves as the foundation of our algorithm. The second methodology employs spectrum curve fitting, wherein the coherent portion of the sideband is excluded, and an appropriate fitting function is applied to extract the incoherent tune. However, within the SAPT context,

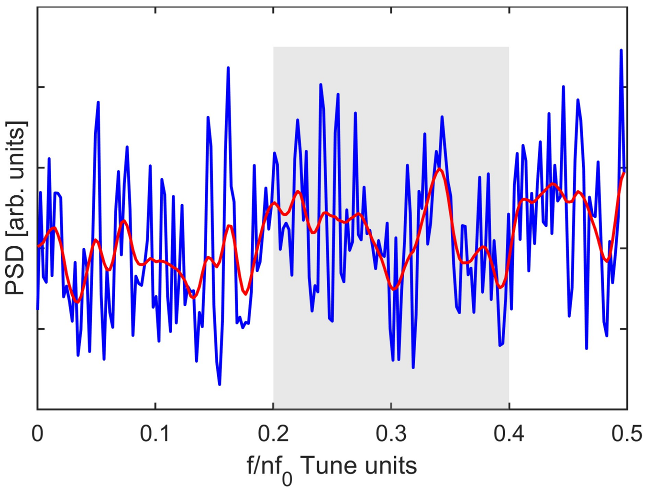

Fig. 5. A Gaussian-weighted average with $\sigma = \frac{N_f-1}{3}$, encompassing 99.7% of the energy within 3σ, is applied to the folded spectrum. The gray-shaded region highlights the frequency range where the transverse sideband is located. The blue line corresponds to the original spectrum, while the red line represents the Gaussian-filtered spectrum.

data collected from the BPM cannot be guaranteed to possess high SNR and frequency resolution, thereby limiting this methodology's applicability to SAPT. The third approach, the Mirrored Difference method, utilizes the coherence between the power of the left and right Bessel p-satellites to determine the precise center of the sidebands. This method, however, proves unsuitable for SAPT applications due to the continuously varying revolution frequency and tune shifting, which precludes the achievement of sufficient frequency resolution required to resolve the internal structure of Bessel satellites.

Experiments in Section IV demonstrate that the original peak-detection algorithm fails to provide satisfactory generalizability and stability under SAPT conditions, particularly in scenarios with low SNR and limited frequency resolution. To address these limitations, we propose an enhanced peak-detection algorithm designed to improve accuracy and stability in challenging low-SNR environments. The algorithm comprises multiple interconnected components, each playing a distinct role in the tune measurement process. The following subsections present these components in detail. It should be noted that, for the sake of clarity in presentation, all evaluations in this section are based on the assumption that the detector has sufficient bandwidth to detect at least one transverse sideband across all energy regions. Cases where certain energy regions cannot be detected will be discussed in Section IV to further demonstrate the robustness of the algorithm.

1. *Exponential Moving Average*

The Exponential Moving Average (EMA) is a widely used statistical technique for smoothing time-series data by assigning exponentially decreasing weights to past observations. Unlike the Simple Moving Average (SMA), which assigns equal weights to all data points within a window, the EMA prioritizes recent data, making it more responsive to recent changes. The EMA at time t is calculated recursively as:

$$\mathrm{EMA}_t = \alpha \cdot x_t + (1-\alpha) \cdot \mathrm{EMA}_{t-1}, \tag{10}$$

where x_t is the current observation, EMA_{t-1} is the previous EMA value, and α $(0 < \alpha \leq 1)$ is the smoothing factor that controls the weight of the current observation. A smaller α results in smoother output, while a larger α emphasizes recent changes. Due to its adaptability and computational efficiency, the EMA is commonly employed in signal processing, financial analysis, and real-time data filtering.

Similarly, the EMA can be applied to accumulate the contribution of the PSDs from past data while emphasizing recent observations. At time t, the current PSD value P_t is computed, and the updated EMA is calculated as:

$$\mathrm{EMA}_t = \alpha \cdot P_t + (1-\alpha) \cdot \mathrm{EMA}_{t-1}. \tag{11}$$

The global maximum's position will serve as the reference tune. This reference tune, along with the tune measured using the WLC method (discussed in Section III C 4), will undergo median filtering (detailed in Section III C 2) to eliminate shot noise interference. These two values represent distinct data points collected from separate sensors for the multi-sensor fusion process.

Given the condition that, in most cases, the betatron tune of SAPT does not undergo abrupt changes, the EMA method can serve as a reliable approach to obtain tune jump, the system can still converge to the new value within tens of milliseconds. The comparison between the reference tune and the nominal tune is presented in Fig. 6.

2. *Online Median Filter*

In the proposed enhanced peak-detection algorithm, the reference tune obtained from EMA is treated as sensor data. In most cases, the observed value can be modeled as sensor data contaminated by Gaussian white noise. However, occasional observations with significant deviations from the actual tune can be attributed to shot noise. To address this, an online median filter is introduced to mitigate the impact of sporadic shot noise. A median filter with an appropriately sized sliding window is applied to perform online filtering on both the reference tune and the measured tune using Weighted Linear Combination (WLC), as discussed in Section III C 4. The results before and after applying the online median filter are illustrated in Fig. 7.

3. *Adaptive Multi-sensor Fusion*

The adaptive multi-sensor fusion framework employs a Kalman filter to integrate the reference tune from Section III C 1 and the measured tune from Section III C 4, treating them as inputs from two sensors. The filter dynamically

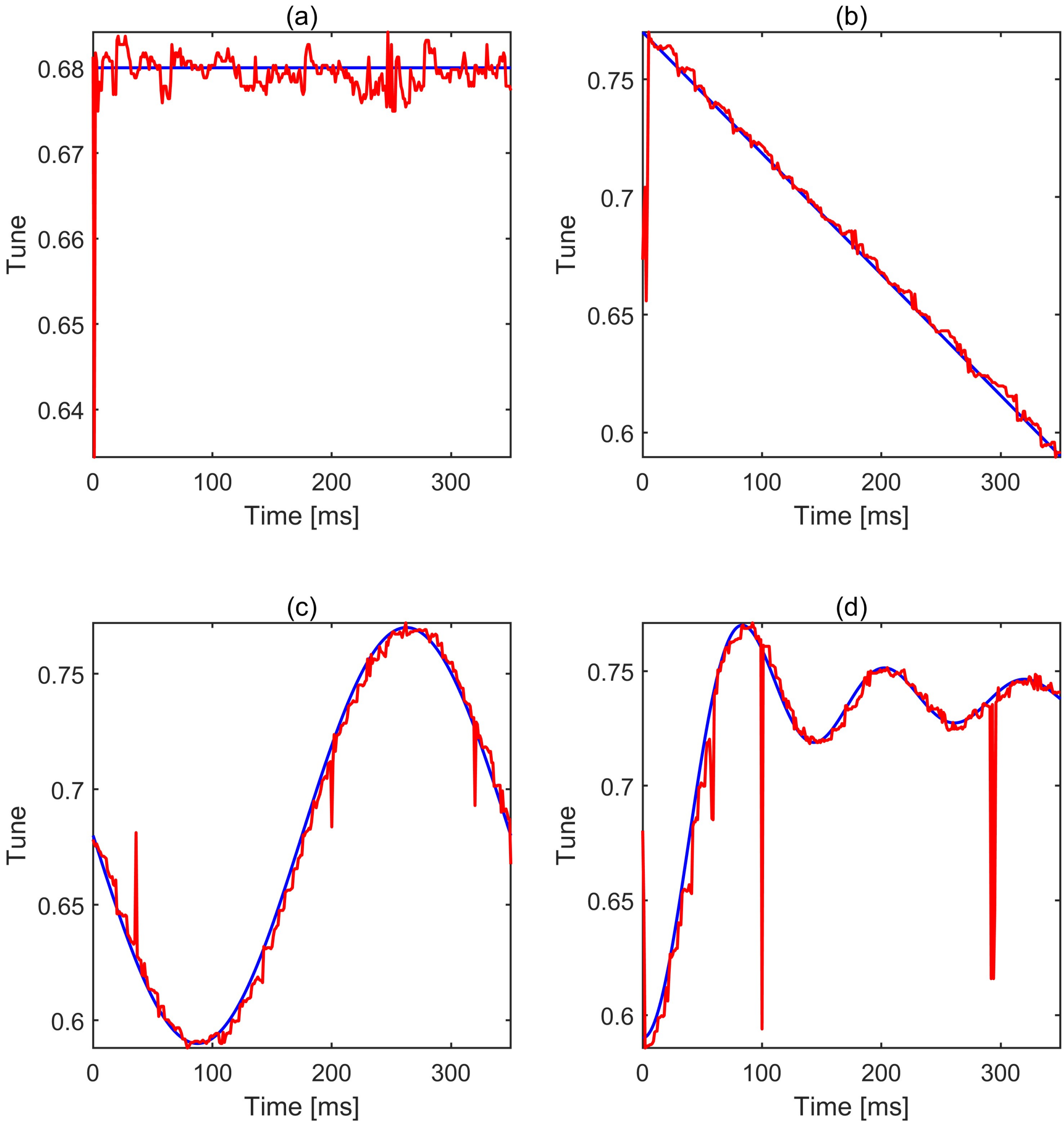

Fig. 6. Comparison between the reference tune (red line), obtained by identifying the global maxima of the EMA result, and the nominal tune (blue line) under different tune shift scenarios. In most cases, the reference tune remains stable and accurate, albeit with slight latency. However, due to strong background noise, occasional fluctuations in the obtained reference tune are observed, which can be attributed to shot noise. The mitigation of these disturbances will be discussed in Section III C 2. It is important to note that the tune variations depicted in the figures are solely intended to evaluate the precision and accuracy of the acquired reference tune and do not represent the actual tune variations of SAPT during operation.

adjusts their contributions based on real-time noise estimation, thereby enhancing the reliability of the state estimate by mitigating the effects of varying measurement noise and occasional shot noise disturbances. The workflow and underlying principles of the adaptive multi-sensor fusion process can be summarized as follows:

- **Initialization:**
  The filter initializes with an initial state estimate x_0 and an associated error covariance P_0. The process noise covariance, Q, accounts for system uncertainties, while the measurement noise covariances, R_1 and R_2, are initially assigned equal fixed values. Additionally, a resid-

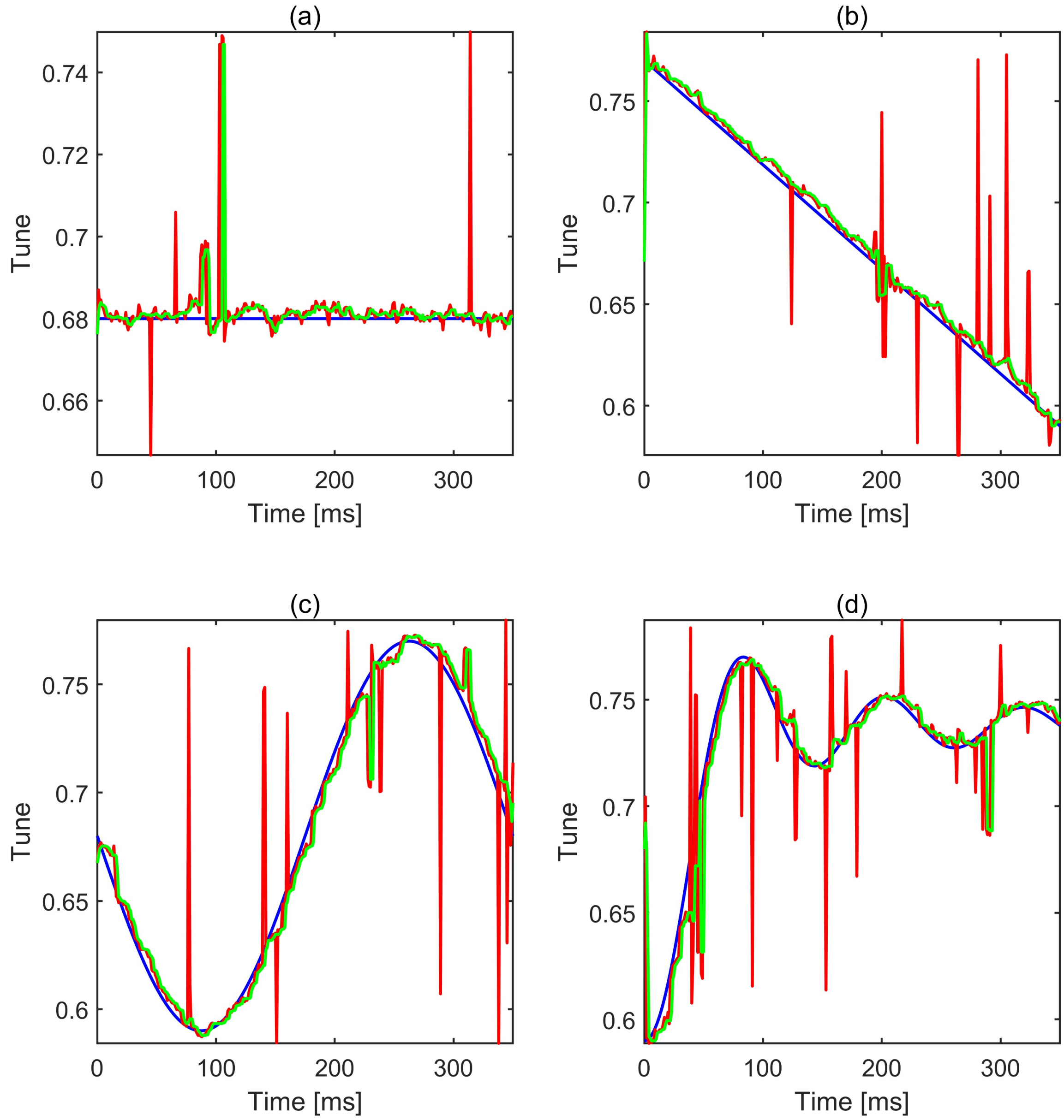

Fig. 7. Comparison of the acquired reference tunes with (green line) and without (red line) online median filtering under different conditions. The blue line represents the nominal tune. The online median filtering process effectively mitigates shot noise in the results; however, it introduces latency, which depends on the filter's window size. It is important to note that the tune variations shown in the figures are solely intended to assess the shot noise reduction capability of the median filter and do not reflect the actual tune variations of SAPT during operation.

ual history window is maintained for each detector to enable dynamic noise estimation.

- **Prediction Step:**
  The prediction step propagates the previous state estimate forward in time under the assumption of an identity state transition model:

$$x_{\text{pred}} = x, \tag{12}$$

$$P_{\text{pred}} = P + Q, \tag{13}$$

where x_{pred} is the predicted state estimate, and P_{pred} is the predicted error covariance incorporating process noise Q.

- **Measurement Fusion:**
  Given two independent measurements, z_1 and z_2, obtained from separate detectors with noise variances R_1 and R_2, their respective precisions are given by:

$$\text{Precision}_1 = \frac{1}{R_1}, \quad \text{Precision}_2 = \frac{1}{R_2}. \tag{14}$$

  The total precision is defined as:

$$\text{Total Precision} = \frac{1}{R_1} + \frac{1}{R_2}. \tag{15}$$

  Using these values, the normalized weights for each detector are computed as:

$$w_1 = \frac{1/R_1}{\text{Total Precision}}, \quad w_2 = \frac{1/R_2}{\text{Total Precision}}. \tag{16}$$

  The fused measurement is then obtained as:

$$z_{\text{fused}} = w_1 z_1 + w_2 z_2, \tag{17}$$

  with the corresponding equivalent measurement noise:

$$R_{\text{fused}} = \frac{1}{\text{Total Precision}}. \tag{18}$$

- **Update Step:**
  The Kalman gain is computed as:

$$K = \frac{P_{\text{pred}}}{P_{\text{pred}} + R_{\text{fused}}}. \tag{19}$$

  The residual (innovation) term for the fused measurement is:

$$\text{Residual}_{\text{fused}} = z_{\text{fused}} - x_{\text{pred}}. \tag{20}$$

  The updated state estimate is then given by:

$$x = x_{\text{pred}} + K \cdot \text{Residual}_{\text{fused}}, \tag{21}$$

  and the error covariance is updated as:

$$P = (1 - K) P_{\text{pred}}. \tag{22}$$

- **Adaptive Noise Estimation:**
  To dynamically adjust the measurement noise, the filter maintains a residual history window (length L) for each detector. The individual residuals are computed as:

$$\text{Residual}_1 = z_1 - x_{\text{pred}}, \tag{23}$$

$$\text{Residual}_2 = z_2 - x_{\text{pred}}. \tag{24}$$

  If and only if the window contains enough residuals, the updated noise estimates for each detector are computed using an exponential smoothing approach:

$$R_i = \alpha \cdot (\text{Residuals}_i)^2 + (1 - \alpha) R_i, \quad i = 1, 2, \tag{25}$$

  where α is the smoothing factor that controls the adaptation rate.

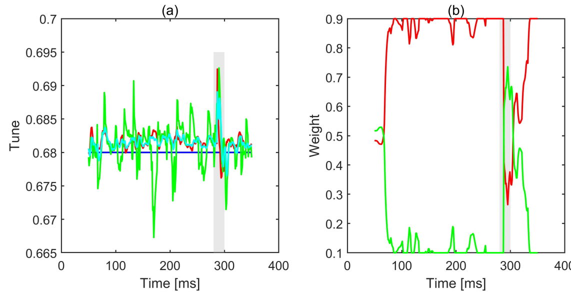

Fig. 8. Fig.8(a) compares the filtered reference tune (red line), filtered measured tune (green line), nominal tune (blue line), and predicted tune (cyan line) under an SNR of -20 dB with $q = 0.68$. Fig.8(b) illustrates the weight variation of the reference tune (red line) and measured tune (green line). The convergence phase is not shown. In most cases, the Kalman filter tends to assign greater confidence to the reference tune, as it is more stable and exhibits fewer fluctuations. However, when inevitable shot noise occurs, as indicated by the gray-shaded region in Fig. 8(a) and 8(b), the weight assigned to the reference tune immediately decreases, prompting the filter to rely more on the measured tune. Once the reference tune stabilizes, the filter gradually restores its weighting preference.

- **Process Noise Update:**
  The process noise covariance is updated based on the squared magnitude of the fused residual:

$$Q = \alpha \cdot (\text{Residual}_{\text{fused}})^2 + (1 - \alpha) Q. \tag{26}$$

  This adaptive approach ensures that the filter dynamically responds to variations in both measurement noise and system uncertainties.

The adaptive multi-sensor fusion mechanism dynamically adjusts the weighting of the reference tune and measured tune, thereby further mitigating the impact of occasional shot noise. When one of the tune signals experiences fluctuations or enters an unstable state, its corresponding weight automatically decreases, indicating that the Kalman filter assigns greater confidence to the data from the other sensor. This dynamic adjustment ensures that the predicted results remain relatively stable, exhibiting lower bias (which enhances accuracy) and reduced standard deviation (which improves robustness), compared to only using online median filter solely for reference tune or measured tune. A comparison of the filtered reference tune, filtered measured tune, nominal tune, and predicted tune using this mechanism is presented in Fig. 8.

4. Weighted Linear Combination

The original peak-detection algorithm is based on the assumption that the SNR is sufficiently high for the transverse sideband to be prominent and easily identifiable. Under this assumption, the highest peak within the designated region is selected as the betatron tune. However, this assumption breaks down when the background noise power significantly exceeds the signal power. In the frequency spectrum, this

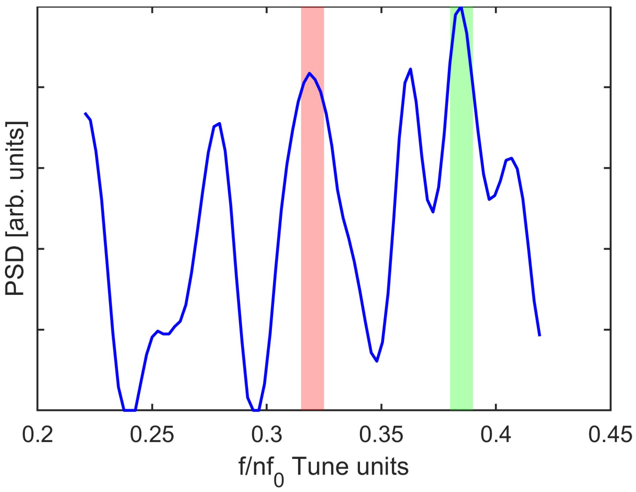

Fig. 9. Folded and smoothed spectrum under an SNR of -20 dB with $q = 0.68$. The peak within the red-shaded region represents the location of true betatron tune; however, it does not exhibit the highest amplitude. The original peak-detection algorithm erroneously identifies the peak within the green-shaded region as the measured tune, as it corresponds to the global maximum in the presented spectrum.

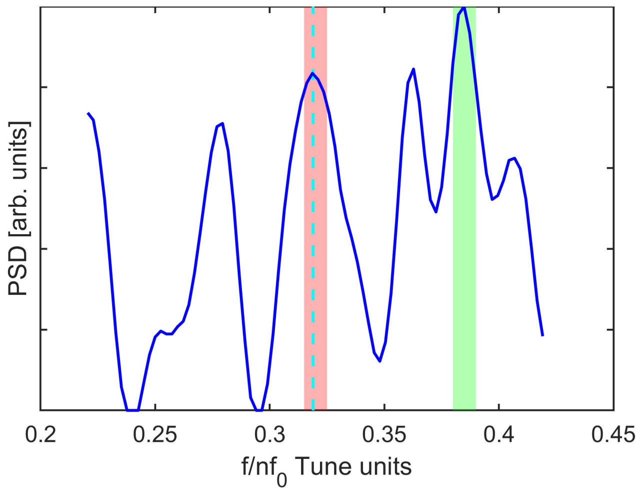

Fig. 10. The peak within the red-shaded region represents the true betatron tune. Relying solely on amplitude would erroneously identify the peak within the green-shaded region as the measured tune, as it corresponds to the global maximum in the presented spectrum. The cyan dashed line represents q_{ref}. Even though the peak in the red-shaded region is not the global maximum, it still receives significant weight because it is the closest local maximum to the reference tune of the previous time step. After applying WLC, the peak in the red-shaded region has the highest confidence and is thus identified as the measured tune.

manifests as multiple peaks of similar amplitude, making it difficult to distinguish the true transverse sideband peak, as illustrated in Fig. 9.

To leverage the temporal continuity of the betatron tune, Weighted Linear Combination (WLC) is introduced to address the limitations of the conventional peak-detection algorithm. WLC is a mathematical operation that combines multiple variables or signals, each multiplied by a corresponding weight. It is widely used in signal processing, optimization, and data analysis to emphasize or de-emphasize the contribution of specific components. The general form of a weighted linear combination is given by:

$$y = \sum_{i=1}^{n} k_i x_i \tag{27}$$

where:

- y is the resulting combined value,
- k_i represents the weight assigned to the i-th component,
- x_i is the i-th input variable or signal,
- n is the total number of components.

The weights k_i are typically normalized such that $\sum_{i=1}^{n} k_i = 1$, ensuring the combination reflects a balanced contribution of all inputs. From Sections III C 1 and III C 2, the reference tune is acquired. Considering that the tune typically does not change abruptly in most cases, we can leverage this property to comprehensively incorporate the tune from the previous time step and the amplitude from the current time step.

Before applying WLC, the locations and amplitudes of all local maxima are identified. Subsequently, two factors are considered. The first factor is the distance between each local maximum and q_{ref}. The distances between all local maxima and q_{ref} are calculated individually, normalized to the range $[0, 1]$, and the corresponding weight is given by

$$P_{\text{distance}} = 1 - \text{distance}. \tag{28}$$

The second factor is the amplitude. The amplitudes of all local maxima are normalized to the range $[0, 1]$, yielding the weight $P_{\text{amplitude}}$.

Next, we introduce a parameter k to represent the weight of P_{distance}, while the weight of $P_{\text{amplitude}}$ is given by $1 - k$. The overall confidence of a local maximum, indicating its likelihood of being the actual tune, is then computed as

$$\text{conf} = k \cdot P_{\text{distance}} + (1 - k) \cdot P_{\text{amplitude}}. \tag{29}$$

The local maximum with the highest confidence is identified as the measured tune. The measured tune is then fed into an adaptive Kalman filter, where all filter parameters are dynamically determined during processing to achieve more stable and consistent results.

WLC leverages the temporal continuity of the tune, assigning greater weight to local maxima that are closer to the tune of the previous time step, rather than relying solely on amplitude. This approach enhances robustness, as shown in Fig. 10.

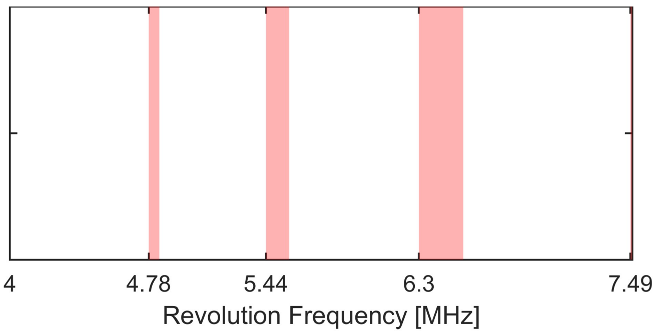

Fig. 11. The red-shaded area represents the frequency region not covered by the BPM at $q = 0.68$. During operation, as the revolution frequency and tune vary dynamically, the uncovered region changes accordingly. This necessitates the post-processing procedure before outputting q_{pred} each time.

D. Post-Processing of Tune Measurement Results

After acquiring q_{pred}, which is the final output of the tune measurement, a post-processing procedure is applied, particularly in cases where the BPM cannot measure the betatron tune across all energy regions or frequency ranges due to bandwidth limitations. Consequently, a validation step is necessary.

The bandwidth of the BPM is denoted as BW_{BPM}, and its operating frequency is represented as f_c. The nearest harmonic to f_c is then determined using:

$$n = \text{round}\left(\frac{f_c}{f_0}\right). \tag{30}$$

Subsequently, we evaluate whether the lower or upper transverse sideband of this harmonic falls within the BPM's bandwidth. If it does not, an **unreliable** flag is transmitted alongside the final output result to the upper-level control system, alerting the control room and other subsystems to potential inaccuracies. An example illustrating the covered and uncovered revolution frequency regions for $q = 0.68$ is shown in Fig. 11.

If the measurement result is relatively reliable, a latency compensation procedure may be applied by adjusting the time stamp of the results forward. This is necessary because the multi-sensor fusion and median filtering introduce system latency, which is directly related to the window size of the median filter. This presents a trade-off between real-time performance and measurement accuracy. Prioritizing real-time performance entirely would make the system more susceptible to shot noise in low SNR environments, potentially leading to inaccurate tune measurements.

E. Overall Workflow

The overall workflow of the proposed betatron tune measurement algorithm can be described as follows:

1. Data Preprocessing:

1.1 The phase-locked loop (PLL) locks and multiplies the RF frequency to an integer multiple, and the output signal is sent to both the FPGA and ADC to ensure synchronized sampling and avoid signal distortion.

1.2 Based on the operating conditions of SAPT, an appropriate STFT window size is determined; these conditions can either be provided by the control room or determined by the FPGA itself based on recent frequency variations.

1.3 The unwanted coherent signal and periodic noise are removed using an RMS fitting method as described in Section III A 2.

2. Tune Measurement:

2.1 After preprocessing, the data are reshaped into multiple batches. The number of frequency bins in each batch is calculated based on the preconfigured minimal frequency resolution and is maintained constant thereafter.

2.2 The power spectral density (PSD) of each batch is calculated, folded, and smoothed, yielding PSD_t, which represents the PSD at time step t. Subsequently, a fixed frequency region covering the expected tune shift range is extracted for further analysis.

2.3 The exponential moving average (EMA) is updated using PSD_t; subsequently, the global maximum is identified and appended to the list L_{ref}. The reference tune, q_{ref}, is computed as the median value of the last N elements of L_{ref} (with N representing an appropriately chosen window size) to mitigate disturbances caused by shot noise.

2.4 The reference tune q_{ref} is treated as the ground truth, while the measured tune, q_{meas}, is obtained by identifying the local maximum with the highest weight using a weighted linear combination (WLC). The resulting measured tune is then processed through a median filter to enhance robustness.

2.5 q_{ref} and q_{meas} are fused using a Kalman filter to produce the final predicted tune, q_{pred}.

3. Post-Processing of Tune Measurement Results

3.1 Given q_{pred} and the current revolution frequency f_0, the FPGA determines whether the combination of q_{pred} and f_0 falls within the BPM's bandwidth. If it does not, an **unreliable** flag is transmitted.

3.2 (Optional) The time stamp of q_{pred} is adjusted forward to compensate for latency.

This system operates in conjunction with SAPT, providing accurate real-time tune measurements across multiple energy regions, regardless of whether the beam is bunched or drifting. A comprehensive evaluation of the algorithm is presented in Section IV.

IV. EXPERIMENTS

The experiments were designed to evaluate and compare the performance of the proposed betatron tune measurement method with the conventional peak-detection algorithm [5, 7] under SAPT conditions. To achieve this, SAPT design parameters were employed in a beam dynamics-based macro-particle simulation, where the revolution frequency was either linearly increased from 4 MHz to 7.5 MHz or held constant, with various types of tune variation introduced and an STFT time window applied. The simulated data were subsequently combined with real noise from the ADC to emulate realistic measurement conditions. In this section, multiple potential application scenarios are considered and analyzed. The analysis compares three key metrics for both the proposed and conventional algorithms: (1) The average absolute error of the measured tune relative to the nominal fractional tune, denoted as μ, which quantifies accuracy; (2) the standard deviation of the measured tune, denoted as σ, which represents stability; and (3) the percentage of measured tunes falling within $q \pm 0.01$ and $q \pm 0.001$, denoted as $P_{q\pm0.01}$ and $P_{q\pm0.001}$, respectively, which evaluate compliance with design requirements. By systematically varying one parameter while keeping the others constant, this analysis provides a comprehensive evaluation of the proposed method's performance relative to the conventional peak-detection algorithm, highlighting its advantages in accuracy and stability under challenging conditions.

All experimental results are acquired through online processing.

A. Scenario 1: Performance under Varying Revolution Frequency and Tune Shift

Assuming the BPM has sufficient bandwidth to capture at least one sideband in each energy region, the revolution frequency and betatron tune of SAPT may not remain constant during operation. The worst-case scenario arises when both parameters vary rapidly, restricting the available sampling time. Although ADC acquisition is triggered by a harmonic of the revolution frequency, an extended sampling duration encompasses a broader frequency range, potentially leading to spectral aliasing and spectral leakage, which can significantly degrade tune measurement accuracy.

This section evaluates the performance of the proposed algorithm in comparison to the conventional peak-detection algorithm. First, either the revolution frequency or the betatron tune is varied while keeping the other parameter fixed under a signal-to-noise ratio (SNR) condition of -20 dB. Subsequently, both the revolution frequency and the betatron tune are varied simultaneously to assess the algorithm's performance under more complex and challenging conditions.

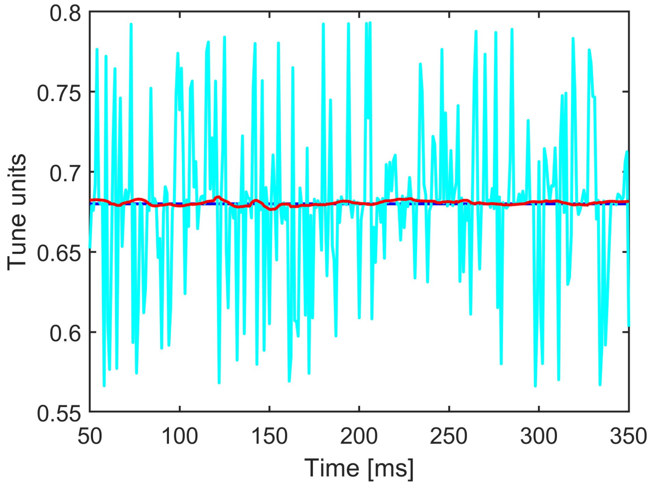

Fig. 12. Comparison of tune measurement results between the proposed algorithm (red line) and the conventional peak-detection algorithm (cyan line), with the nominal tune shown as the blue line. The figure demonstrates that the conventional peak-detection algorithm fails to accurately identify the betatron tune in low-SNR environments. A more detailed comparison of the performance of the proposed algorithm and the conventional peak-detection algorithm will be presented in Section IV D.

Table 2. Comparison of the average absolute error (μ) of the measured tune relative to the nominal fractional tune q, standard deviation (σ) of the measured tune, and the percentage of measured tunes falling within $q \pm 0.01$ ($P_{q\pm0.01}$) and $q \pm 0.001$ ($P_{q\pm0.001}$) for proposed algorithm and conventional peak-detection algorithm. The comparison is performed under an SNR of -20 dB.

Method	μ	σ	$P_{q\pm0.001}$	$P_{q\pm0.01}$
Peak Detection [5]	0.0327	0.0371	13.29%	48.50%
Proposed Algorithm	0.0012	0.0009	46.51%	100.00%
Proposed Algorithm (latency compensated)	0.0012	0.0009	46.51%	100.00%

1. *Varying Revolution Frequency*

The revolution frequency increases linearly from 4 MHz to 7.5 MHz, following the trend illustrated in Fig. 2, while the betatron tune remains constant at $q = 0.68$ under an SNR of -20 dB. The STFT time window size is set to 1 ms to address the rapid increase in revolution frequency and to avoid significant spectrum aliasing, leakage and bias. The comparison of tune measurement results is presented in Fig. 12, while the corresponding values of μ, σ, $P_{q\pm0.01}$, and $P_{q\pm0.001}$ for both the proposed method and the conventional peak-detection algorithm are summarized in Table 2. The conventional peak-detection algorithm was unable to accurately measure the betatron tune under low SNR conditions; consequently, the subsequent experiments will exclusively present graphical representations of the proposed algorithm's performance, while the numerical comparison between the conventional peak-detection algorithm and the proposed algorithm will be summarized in tabular form.

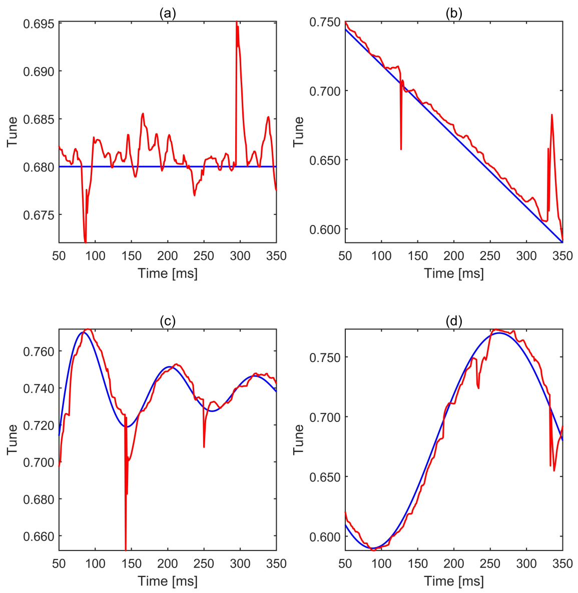

Fig. 13. Comparison of tune measurement results between the proposed algorithm (red line) and the nominal tune (blue line) for four different types of tune shifts.

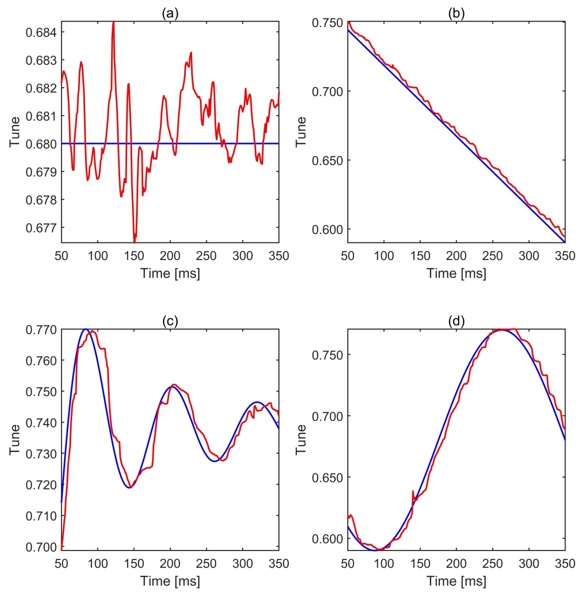

Fig. 14. Comparison of tune measurement results between the proposed algorithm (red line), with the nominal tune shown as the blue line.

Table 3. Comparison of overall performance metrics for tune measurement methods at -20 dB SNR across four tune shift patterns.

Method	μ	σ	$P_{0.001}$	$P_{0.01}$
Peak Detection [5]	0.0452	0.0470	4.98%	32.87%
Proposed Algorithm	0.0073	0.0090	11.45%	80.28%
Proposed Algorithm (latency compensated)	0.0056	0.0086	17.73%	87.65%

[a] μ: average absolute error; σ: standard deviation; $P_{0.001}$: percentage of tunes within $q \pm 0.001$; $P_{0.01}$: percentage within $q \pm 0.01$.

Table 4. Comparison of tune measurement methods at -20 dB SNR across four tune shift patterns.

Method	μ	σ	$P_{0.001}$	$P_{0.01}$
Peak Detection [5]	0.0467	0.0479	5.28%	34.26%
Proposed Algorithm	0.0054	0.0066	18.13%	85.56%
Proposed Algorithm (latency compensated)	0.0035	0.0060	27.39%	95.92%

[a] μ: average absolute error relative to nominal tune q; σ: standard deviation; $P_{0.001}$, $P_{0.01}$: percentage of measurements within $q \pm 0.001$ and $q \pm 0.01$, respectively.

2. *Tune Shift*

The revolution frequency will be maintained at a constant value of 7.5 MHz, while the tune is varied in different ways. The performance of the proposed algorithm under an SNR of -20 dB is illustrated in Fig. 13, while the numerical comparison between the proposed algorithm and the conventional peak-detection algorithm is presented in Table. 3. It should be noted that the presented tune variations are solely intended to evaluate the performance of the algorithm and do not represent the actual tune variations during operation.

3. *Varying Revolution Frequency and Tune Shift*

During ramping, the simultaneous increase in revolution frequency and tune shift limits the available sampling time. The STFT time window size is set to 1 ms, as described in Section IV A 1. The performance and numerical comparison are presented in Fig. 14 and Table 4.

B. Scenario 2: Performance under Data Contamination and Signal Loss

During daily operation, unexpected disturbances or hardware limitations may introduce strong noise into the ADC-acquired data or result in the complete absence of transverse signal content. The latter scenario occurs in SAPT because the bandwidth of the developing detector is insufficient to cover all energy regions during ramping or extraction. In this case, the transverse sideband may not appear in the spectra, leaving only noise. Consequently, it is crucial to assess the algorithm's ability to converge to the actual tune value after being affected by disturbances. The performance under data contamination or signal loss, with a revolution frequency of 7.5 MHz, an SNR of -20 dB, and a 1 ms STFT time window, is illustrated in Fig. 15. Given a 1 ms STFT time window, the

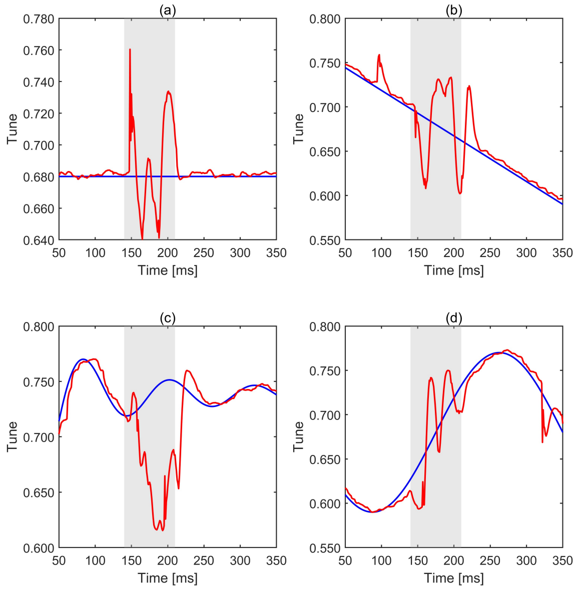

Fig. 15. Comparison of performance between the proposed algorithm (red line) and the nominal tune (blue line) under data contamination and signal loss. The gray-shaded area represents the region where no transverse sideband is present, and only noise exists. After exiting the contamination zone, the algorithm requires approximately 20 ms to converge to the actual tune.

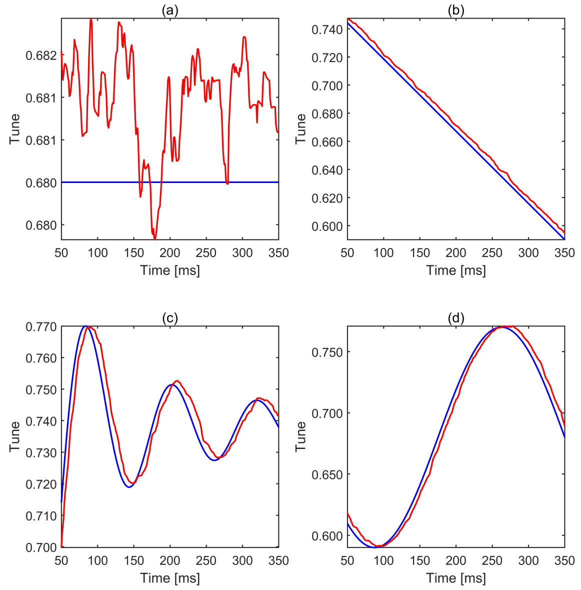

Fig. 16. Comparison of the performance between the proposed algorithm (red line) and the nominal tune (blue line) under a relatively stable revolution frequency and a longer sampling time. Occasional shot noise is no longer present due to the summation of more batches, which increases the SNR.

measured results converge to the actual value in less than 50 ms.

C. Scenario 3: Performance under Relatively Stable Revolution Frequency

If the revolution frequency remains stable, it is practical to use a longer sampling time, such as 10 ms, to achieve more precise tune measurements. This approach also mitigates the influence of shot noise in low-SNR environments. The performance of the proposed algorithm, along with numerical metrics, is compared with the conventional peak-detection algorithm in Fig. 16 and Table 5.

D. Scenario 4: Performance under the Absence of Coherent Tune

During SAPT operation, obtaining a coherent tune signal from BPM data is challenging. Therefore, it is essential to evaluate the algorithm's performance in the absence of a coherent tune signal. The noise amplitude is calculated based on the signal containing a coherent component, after which the coherent signal content is removed using the method described in Section III A 2. The remaining signal is then combined with noise. Experimental results indicate that the absence of a coherent tune signal slightly increases the minimum SNR required for accurate tune measurement. However, at an SNR of -15 dB, the algorithm still demonstrates good accuracy with relatively low error, as shown in Fig. 17 and Table 6.

Table 5. Comparison of the overall average absolute error (μ) of the measured tune relative to the nominal fractional tune q, standard deviation (σ) of the measured tune, and the percentage of measured tunes falling within $q \pm 0.01$ ($P_{q\pm0.01}$) and $q \pm 0.001$ ($P_{q\pm0.001}$) for the proposed algorithm and the conventional peak-detection algorithm under stable revolution frequency and tune shift conditions. The comparison is conducted at an SNR of -20 dB across four different types of tune shifts.

Method	μ	σ	$P_{q\pm0.001}$	$P_{q\pm0.01}$
Peak Detection [5]	0.0092	0.0219	18.82%	87.55%
Proposed Algorithm	0.0041	0.0030	17.33%	95.32%
Proposed Algorithm (latency compensated)	0.0017	0.0012	36.45%	100.00%

E. Scenario 5: Performance under Different SNR

The SNR of the acquired signal is influenced by multiple factors. To ensure the generalization and accuracy of the proposed method, it is essential to evaluate its performance across different SNR values. The comparison between the proposed algorithm and the conventional peak-detection algorithm is illustrated in Fig. 18, while the numerical results

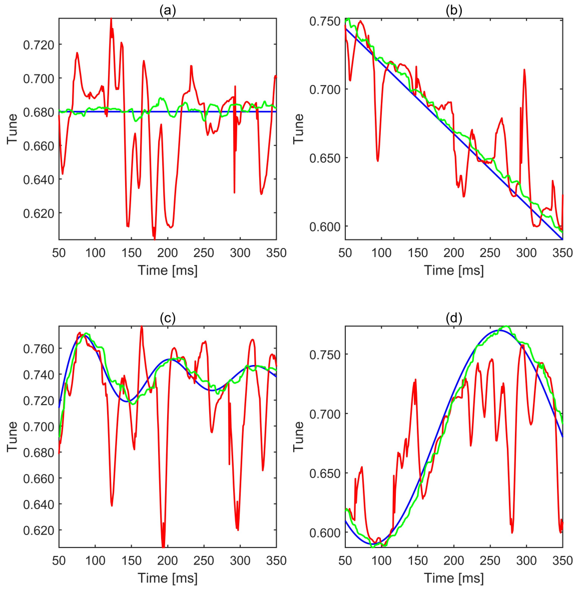

Fig. 17. Comparison of the performance of the proposed algorithm under -20 dB SNR (red line) and -15 dB SNR (green line), with the nominal tune shown as the blue line. The absence of a coherent signal reduces the power of the transverse sideband, thereby increasing the minimum SNR required for accurate tune measurement.

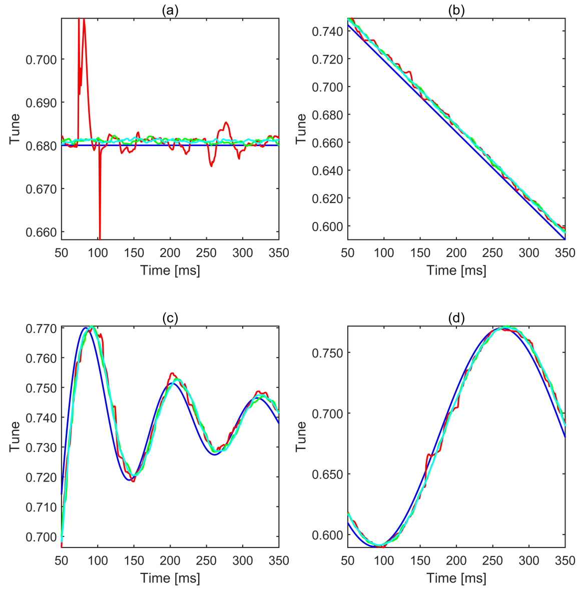

Fig. 18. Comparison of the performance of the proposed algorithm under -20 dB SNR (red line), -15 dB SNR (green line) and -10 dB SNR (cyan line), with the nominal tune shown as the blue line.

Table 6. Comparison of the overall average absolute error (μ) of the measured tune relative to the nominal fractional tune q, standard deviation (σ) of the measured tune, and the percentage of measured tunes falling within $q \pm 0.01$ ($P_{q\pm0.01}$) and $q \pm 0.001$ ($P_{q\pm0.001}$) for the proposed algorithm and the conventional peak-detection algorithm under stable revolution frequency and tune shift conditions. The comparison is conducted at an SNR of -15 dB across four different types of tune shifts.

Method	$\boldsymbol{\mu}$	$\boldsymbol{\sigma}$	$\boldsymbol{P_{q\pm0.001}}$	$\boldsymbol{P_{q\pm0.01}}$
Peak Detection [5]	0.0374	0.0436	3.98%	36.85%
Proposed Algorithm	0.0057	0.0044	11.45%	85.76%
Proposed Algorithm (latency compensated)	0.0042	0.0034	15.94%	94.72%

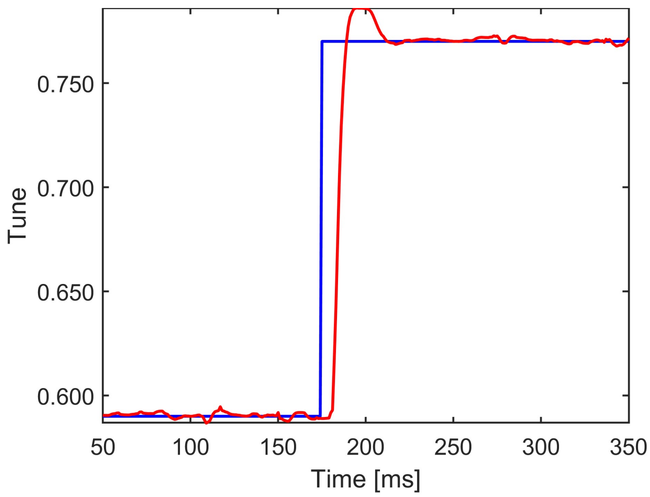

Fig. 19. Comparison of the proposed algorithm's performance under a tune jump scenario. The measured results are represented by the red line, while the nominal tune is depicted by the blue line. Following the tune jump, after a brief latency, the measured results rapidly converge to the actual tune value and remain stable. The entire process takes less than 50 ms.

are presented in Table 7.

F. Scenario 6: Performance under Tune Jump

During operation, tune jumps may occur. These abrupt changes in betatron tune require the tune measurement system to detect such events, rather than classify them as outliers, and to converge to the actual value as quickly as possible while maintaining accuracy and precision.

To evaluate the proposed algorithm's ability to handle this scenario, experiments were conducted under an SNR of -20 dB with an STFT time window of 1 ms to assess the algorithm's performance under the worst conditions in which it can operate.

The performance results are shown in Fig. 19.

G. Results Discussion

The experimental results demonstrate the superior performance of the proposed betatron tune measurement algorithm

Table 7. Comparison of the average absolute error (μ) of the measured tune relative to the nominal fractional tune q, standard deviation (σ) of the measured tune, and the percentage of measured tunes falling within $q \pm 0.01$ ($P_{q\pm0.01}$) and $q \pm 0.001$ ($P_{q\pm0.001}$) for the proposed algorithm and the conventional peak-detection algorithm under stable revolution frequency and tune shift conditions across SNR conditions of -20 dB, -15 dB and -10 dB.

SNR	Method	μ	σ	$P_{q\pm0.001}$	$P_{q\pm0.01}$
	Peak Detection [5]	0.0452	0.0470	4.98%	32.87%
-20 dB	Proposed Algorithm	0.0073	0.0090	11.45%	80.28%
	Proposed Algorithm (latency compensated)	0.0056	0.0086	17.73%	87.65%
	Peak Detection [5]	0.0121	0.0268	17.23%	80.88%
-15 dB	Proposed Algorithm	0.0039	0.0029	14.94%	96.71%
	Proposed Algorithm (latency compensated)	0.0016	0.0012	37.85%	100.00%
	Peak Detection [5]	0.0024	0.0020	28.98%	99.40%
-10 dB	Proposed Algorithm	0.0039	0.0028	15.74%	97.71%
	Proposed Algorithm (latency compensated)	0.0014	0.0010	40.14%	100.00%

compared to the conventional peak-detection method under various challenging conditions. The findings are summarized as follows:

1. Performance under Varying Revolution Frequency and Tune Shift

- The proposed algorithm effectively tracks betatron tune variations even when the revolution frequency changes at a rate of approximately 10 MHz/s.
- Under an SNR of -20 dB, the conventional peak-detection algorithm exhibits reduced accuracy due to strong noise spectrum interference, whereas the proposed algorithm maintains significantly lower error and higher stability.
- When both the revolution frequency and tune shift occur simultaneously, the proposed method continues to provide reliable measurements, demonstrating robustness in complex scenarios.

2. Performance under Data Contamination and Signal Loss

- The proposed algorithm successfully converges to the actual tune value after disturbances, with convergence occurring within 50 ms.

3. Performance under Relatively Stable Revolution Frequency

- With a longer sampling duration, the proposed algorithm achieves enhanced precision, benefiting from improved frequency resolution and reduced noise influence.
- The statistical results indicate that increasing the sampling duration significantly improves measurement stability while maintaining responsiveness to tune variations.

4. Performance in the Absence of a Coherent Tune Signal

- The removal of the coherent signal slightly increases the minimum required SNR for accurate tune measurements.
- Nevertheless, at an SNR of -15 dB, the proposed algorithm maintains relatively low measurement error, confirming its applicability even in the absence of a strong coherent tune signal.

5. Performance under Different SNR Conditions

- As the SNR improves from -20 dB to -10 dB, the accuracy and precision of the proposed method steadily increase.
- The algorithm consistently outperforms the conventional peak-detection method, particularly in low-SNR environments, where traditional methods exhibit severe degradation.

6. Performance under Tune Jumps

- The algorithm successfully detects abrupt tune jumps and rapidly converges to the actual tune value within 50 ms.
- The proposed method correctly identifies these jumps as genuine changes and maintains accuracy and stability after convergence.

H. Summary of Experimental Findings

The experimental results confirm that the proposed betatron tune measurement algorithm offers superior accuracy, stability, and robustness across diverse operational conditions. Its ability to handle rapid frequency variations, noise contamination, signal loss, and abrupt tune jumps makes it

a reliable alternative to conventional methods, particularly in low-SNR environments.

V. LIMITATIONS AND FUTURE WORK

The resonant stripline BPM for betatron tune measurement is still under development, making it currently infeasible to detect the Schottky signal and validate the proposed algorithm on the existing SAPT facility. Additionally, the BPM's performance remains uncertain. To address this limitation, the proposed algorithm was evaluated through macro-particle simulations incorporating realistic beam dynamics models based on SAPT design parameters and actual ADC noise, ensuring that the simulated conditions closely resemble real experimental environments. The validation under an SNR as low as -20 dB, as discussed in Section IV, was conducted to account for potential BPM performance constraints in practical applications.

Once the BPM is fully developed, manufactured, and installed on SAPT or another synchrotron for proton therapy, the proposed algorithm will undergo rigorous testing with real experimental data. The evaluation will include direct comparisons with conventional tune measurement methods to assess accuracy and robustness in an operational setting. If BPM development is delayed, alternative validation strategies, such as testing on existing BPM systems with partial implementation, will be explored to provide additional experimental support.

VI. CONCLUSION

In this paper, we proposed a novel Schottky diagnostics-based method for real-time betatron tune measurement in SAPT. The method addresses critical challenges such as low SNR, varying revolution frequency, and fluctuating betatron tune. By leveraging macro-particle beam-dynamics simulations and incorporating real-world noise, we demonstrated the method's capability to extract transverse Schottky signals from noisy environments. The proposed approach utilizes STFT combined with advanced smoothing and signal processing techniques to achieve accurate betatron tune measurements under a wide range of experimental conditions.

Experimental results demonstrate that the proposed method significantly outperforms the conventional peak-detection algorithm in terms of precision, accuracy, and robustness. The method achieves an average absolute error (μ) relative to the nominal fractional tune of less than 0.01, with a low standard deviation (σ), thereby meeting the stringent design requirements for high-accuracy tune diagnostics. These results highlight the method's general applicability and stability, even under challenging operational scenarios such as rapid frequency ramping, tune shifts, and low SNR conditions.

This study lays the groundwork for optimizing betatron tune diagnostics in ramping synchrotrons and advancing diagnostic techniques for applications such as proton therapy. Future work will focus on expanding the operational range of the proposed method and validating its applicability in other synchrotron facilities. Additionally, efforts will be directed toward further optimizing computational efficiency to enhance real-time performance in demanding environments.

To facilitate practical implementation, an FPGA-based online system for the proposed method is currently under development. This system aims to provide high-accuracy, real-time betatron tune measurements for SAPT, further enhancing the diagnostic capabilities of modern synchrotron facilities.

VII. BIBLIOGRAPHY

[1] F. Nolden, Instrumentation and diagnostics using Schottky signals. Proc. DIPAC 01, 6 (2001).

[2] C. Lannoy, K. Lasocha, T. Pieloni, *et al.*, Impact of beam-coupling impedance on the Schottky spectrum of bunched beam. Journal of Instrumentation, **19**(03): P03017 (2024). doi: 10.1088/1748-0221/19/03/P03017

[3] M.-Z. Zhang, D.-M. Li, L.-R. Shen, *et al.*, SAPT: a synchrotron-based proton therapy facility in Shanghai. Nuclear Science and Techniques, **34**(10): 148 (2023). doi: 10.1007/s41365-023-01246-8

[4] S. van der Meer, Stochastic damping of betatron oscillations in the ISR. CERN, CERN-ISR-PO-72-31, ISR-PO-72-31, Geneva (1972). URL: https://cds.cern.ch/record/312939

[5] M. Betz, O.R. Jones, T. Lefevre, *et al.*, Bunched-beam Schottky monitoring in the LHC. Nuclear Instruments and Methods in Physics Research Section A: Accelerators, Spectrometers, Detectors and Associated Equipment, **874**: 113–126 (2017). doi: 10.1016/j.nima.2017.08.045

[6] S. Van der Meer, Diagnostics with Schottky noise. CERN, CERN-PS-88-60-AR, Geneva (1988). URL: https://cds.cern.ch/record/2844075

[7] O. Chanon, Schottky signal analysis: tune and chromaticity computation. Technical Report (2016).

[8] K. Lasocha, D. Alves, Estimation of longitudinal bunch characteristics in the LHC using Schottky-based diagnostics. Physical Review Accelerators and Beams, **23**(6): 062803 (2020). doi: 10.1103/PhysRevAccelBeams.23.062803

[9] K. Lasocha, D. Alves, Estimation of transverse bunch characteristics in the LHC using Schottky-based diagnostics. Physical Review Accelerators and Beams, **25**(6): 062801 (2022). doi: 10.1103/PhysRevAccelBeams.25.062801

[10] K. Łasocha, Non-Invasive Beam Diagnostics with Schottky Signals and Cherenkov Diffraction Radiation. PhD Thesis (2022).

[11] R.G. Vaughan, N.L. Scott, D.R. White, The theory of bandpass sampling. IEEE Transactions on signal processing, **39**(9): 1973–1984 (1991). doi: 10.1109/78.134430

[12] D. Boussard, Schottky noise and beam transfer function diagnostics. CERN (1986).

[13] P.J. Rousseeuw, C. Croux, Alternatives to the median absolute deviation. Journal of the American Statistical association, **88**(424): 1273–1283 (1993). doi:

10.1080/01621459.1993.10476408

[14] W.S. Cleveland, Robust locally weighted regression and smoothing scatterplots. Journal of the American statistical association, **74**(368): 829–836 (1979). doi: 10.1080/01621459.1979.10481038

[15] C. Lannoy, D. Alves, K. Łasocha, *et al.*, LHC Schottky spectrum from macro-particle simulations. In: 11th International Beam Instrumentation Conference, 308–312 (2022).

[16] G. Iadarola, R. De Maria, S. Lopaciuk, *et al.*, Xsuite: An integrated beam physics simulation framework. arXiv preprint arXiv:2310.00317 (2023).

[17] R.W. Schafer, What is a savitzky-golay filter? IEEE Signal processing magazine, **28**(4): 111–117 (2011). doi: 10.1109/MSP.2011.941097

[18] K. Łasocha, D. Alves, C. Lannoy, *et al.*, Extraction of LHC Beam Parameters from Schottky Signals. JACoW HB, **2023**: 382-388 (2024). doi: 10.18429/JACoW-HB2023-THC2I2

[19] A. Savitzky, M.J.E. Golay, Smoothing and differentiation of data by simplified least squares procedures. Analytical chemistry, **36**(8): 1627–1639 (1964). doi: 10.1021/ac60214a047

[20] B. Keil, A. Citterio, M. Dehler, *et al.*, Commissioning of the low-charge resonant stripline BPM system for the SwissFEL test injector. Proc. FEL, 429 (2010).

[21] A. Citterio, M. Dehler, D.M. Treyer, *et al.*, Design of a Resonant Stripline Beam Position Pickup for the 250MeV PSI XFEL Test Injector. Proc. DIPAC, Vol. 9 (2009).

[22] T. Petersen, J. Diamond, N. Liu, *et al.*, Fermilab Switchyard Resonant Beam Position Monitor Electronics Upgrade Results. arXiv preprint arXiv:1701.00816 (2017).

[23] M. Kesselman, P. Cameron, J. Cupolo, Resonant BPM for Continuous Tune Measurement in RHIC. PACS2001. Proceedings of the 2001 Particle Accelerator Conference, **2**: 1357–1359 (2001).

[24] M. Dehler, Resonant strip line BPM for ultra low current measurements. Proc. DIPAC, **5**: 284 (2005).